Environmental Science

Nano

ROYAL SOCIETY
OF **CHEMISTRY**

PAPER
Gloria B. Ramírez-Rodríguez, José M. Delgado-López *et al.*
Nanoelicitors with prolonged retention and sustained release
to produce beneficial compounds in wines

PAPER

Check for updates

Nanoelicitors with prolonged retention and sustained release to produce beneficial compounds in wines†

Belén Parra-Torrejón, [iD] [a] Gloria B. Ramírez-Rodríguez, [iD] *[a]
Maria J. Giménez-Bañón,[b] Juan D. Moreno-Olivares,[b]
Diego F. Paladines-Quezada, [iD] [b]
Rocío Gil-Muñoz[b] and José M. Delgado-López [iD] *[a]

Methyl jasmonate (MeJ), an elicitor able to trigger plant defence responses, is a natural and clean alternative to the use of hazardous pesticides. However, the efficient application of MeJ in fields is very limited due to its poor water solubility, thermal stability and phytotoxicity at the high dose required to produce beneficial effects in plants. Here, a novel nanoelicitor (nano-MeJ) was prepared through the functionalization of biocompatible calcium phosphate nanoparticles. The resulting nanocomposite produced a significant increase of beneficial compounds (phytoalexins) in grapes and wines at low MeJ dosage. Indeed, results from *in vivo* field experiments on Monastrell vineyards (*Vitis vinifera* L.) revealed that grapes treated with nano-MeJ provided red wines with high content of beneficial stilbenes, similar to the levels obtained with conventional treatments but applying 10 times higher MeJ dosage. We demonstrated that the nanoparticles protect and retain MeJ on the surface of the leaves over long periods of time. This protective action along with the slow release provides a prolonged supply of the resistance-inductor elicitor through the leaves, resulting in a significant efficiency increase. Additionally, the nanocomposite was stable for long periods of time (more than 175 days) and exhibited lower cytotoxicity compared to MeJ, which are important features for its efficient and safe use in agriculture.

Environmental significance

Inefficient application of pesticides and agrochemicals has caused serious environmental damage. Elicitors, like methyl jasmonate (MeJ), able to induce plant defence responses to biotic and abiotic stresses, are clean and promising alternatives. However, their poor thermal stability and low solubility in water hinder their efficient use in fields. To overcome this issue, we have designed a clean and safe nanocomposite, which provides a gradual release and protects the elicitor on the leaves over longer periods of time. By means of *in vivo* field experiments, we found a significant (ten-fold) efficiency increase with the foliar application of the nanoparticles in grapevines. These engineered nanocomposites are promising alternatives to pesticides for sustainable plant pest management and the concomitant increase of the quality of fruits.

Introduction

The use of pesticides and agrochemicals has resulted in a noticeable increase in food production and crop yields over the last few decades. However, more than 99% of applied pesticides are either lost in the surrounding environment or unable to reach the target area due to leaching, evaporation, deposition and/or degradation by photolysis, hydrolysis and microbial activity.[1] Owing to this, the concentration of active ingredients in pesticides is far below the minimum effective concentration, thus requiring repeated applications. This indiscriminate use causes significant environmental damage such as water pollution, soil contamination, increased pest and pathogen resistance and loss of biodiversity, among others.[1,2]

As an alternative, the self-protection mechanisms that plants have evolved against biotic and abiotic stresses are being used as a source of inspiration to develop eco-friendly formulations. Elicitors induce structural and/or biochemical responses associated with the expression of plant disease resistance and have been proposed as potential alternatives

[a] *Departamento de Química Inorgánica, Facultad de Ciencias, Universidad de Granada, Av. Fuente Nueva, s/n, 18071 Granada, Spain. E-mail: gloria@ugr.es, jmdl@ugr.es*
[b] *Instituto Murciano de Investigación y Desarrollo Agroalimentario, Ctra. La Alberca s/n, 30150, Murcia, Spain*
† Electronic supplementary information (ESI) available. See DOI: 10.1039/d1en00504a

3524 | *Environ. Sci.: Nano*, 2021, **8**, 3524–3535

This journal is © The Royal Society of Chemistry 2021

for effective management of plant diseases.[3] Among them, methyl jasmonate (MeJ) or its acidic derivative (jasmonic acid) is a hormone, widely found in the plant kingdom, involved in plant signalling.[3,4] MeJ stimulates the synthesis of defensive compounds and initiates the expression of pathogenesis-related genes involved in systemic acquired resistance and local resistance.[4] This induces plant defences against herbivore attack and pathogen infection, and confers tolerance to abiotic stresses such as salinity, drought, high and low temperatures, heavy metals, ozone and ultraviolet radiation.[5,6] In addition, MeJ induces positive effects on diverse developmental processes of plants including seed germination, root growth, stamen development, flowering, fruit ripening, and leaf senescence[5,6] and enhances the yields and quality parameters of a large variety of fruits.[7–11]

One of the defence mechanisms of plants against pests and pathogens is the production of low molecular mass secondary metabolites (i.e., phytoalexins) with antimicrobial activity, such as anthocyanins, stilbenes, and flavonols.[7,12–15] These phenolic compounds are also the major responsible for the organoleptic properties of wine and grapes, including the wine colour, mouth feel properties and aging potential and stability.[14] Concretely, trans-resveratrol (3,5,4′-trihydroxy-trans-stilbene) has received widespread attention owing to its anti-inflammatory, anti-carcinogenic and cardio-protective properties. It is indeed considered as one of the major responsible for the health benefits associated with red wines.[16–19] Numerous experimental trials with different elicitors have been conducted to promote stilbene synthesis in grapevine berries, with MeJ being the elicitor providing the highest concentration of these beneficial compounds in Monastrell grapes.[20] Nonetheless, the enrichment of wines in beneficial polyphenols requires a high concentration of MeJ (ca. 10 mM) to be applied through the leaves during veraison.[7,12–15] Unfortunately, the low water solubility, poor thermal stability and phytotoxicity of MeJ limit its efficient applicability, particularly at such a high concentration.[21,22] Therefore, smarter materials able to protect the elicitor and prolong its retention on the leave surface are needed to provide sustained and more efficient administration.

In this line, the introduction of nanotechnology in agriculture provides multiple benefits over conventional agrochemicals such as controlled release kinetics, enhanced permeability and solubility and prevention of premature degradation under harsh environmental conditions.[1,23,24] Nanocarriers are indeed potential tools to reduce the pesticide dosage allowing sustainable pest management.[24] A recent study reported the first application of a nano-delivery system of an elicitor (i.e., chitosan) to improve plant defense.[25] The nano-sized chitosan/star polycation complexes exhibited enhanced control effects against potato late blight.[25] Nanomaterials have been also exploited as a novel generation of post-harvest technology to reduce the utilization of synthetic fungicides to control post-harvest rot in fruits such as grapes, citrus, bananas, apples, mangos, peaches, and nectarines.[26] In the case of table grapes (Vitis vinifera L.), recent research studies demonstrated that nanomaterials such as silica, chitosan or the combination of both nanoparticles are promising compounds for management of gray mold.[26]

Among the wide variety of engineered nanosystems, calcium phosphate nanoparticles, the major constituent of bones and teeth in vertebrates (i.e., nanocrystalline apatite (Ap) and its ephemeral precursor amorphous calcium phosphate (ACP)), have been long proposed as ideal nanocarriers in nanomedicine due to their inherent biocompatibility and biodegradability.[27,28] Moreover, their high capability to be doped with foreign ions or molecules (e.g., K^+, Mg^{2+}, Zn^{2+}, CO_3^{2-}, NO_3^-, urea, etc.) and tuneable solubility make them an ideal nanoplatform to provide sustained delivery of multiple nutrients upon nanoparticle dissolution.[29–31] In fact, several studies in the agrochemical field demonstrated the potential of ACP and Ap nanoparticles for the controlled delivery of plant macronutrients, such as phosphorus[32–38] and nitrogen.[29,30,39–42] Synthetic Ap nanoparticles have been also functionalized with humic substances (HS) providing the synergistic co-release of crop nutrients and stimulants. A pot test in Zea mays as a crop model demonstrated that this multifunctional nanofertilizer leads to a significant improvement of crop nutrition, resistance to NaCl-induced abiotic stresses and rhizosphere bacteria growth.[43] Calcium phosphate particles recovered from food by-products rich in phosphorus such as fish bone (i.e., Sardinella aurita or Salmo salar) have been successfully used as a fertilizer and this has been proposed as a potential strategy for the circular economy of phosphorus.[44,45]

In this work, we developed a more efficient and safer treatment of MeJ, based on the use of ACP nanoparticles, which provide protective action and slow delivery of the elicitor. Firstly, we optimized the functionalization of ACP nanoparticles with MeJ and evaluated its cytotoxicity, stability and release kinetics. The efficiency of nano-MeJ in comparison to that of conventional treatments was demonstrated by means of in vivo field experiments on Monastrell (Vitis vinifera L.) vineyards. Concretely, we studied the content of beneficial stilbenes in wines obtained from grapes harvested after different treatments. In addition, in vitro assays were carried out with the aim of explaining the interesting results of in vivo field experiments.

Materials and methods

Materials

Sodium citrate tribasic dihydrate ($Na_3(C_6H_5O_7) \cdot 2H_2O$, ≥99.0% pure), potassium phosphate dibasic anhydrous (K_2HPO_4, ≥99.0% pure), sodium carbonate (Na_2CO_3, ≥99.0% pure), calcium nitrate tetrahydrate ($Ca(NO_3)_2 \cdot 4H_2O$, ≥99.0% pure) and methyl jasmonate ($C_{13}H_{20}O_3$, 95.0%, racemic) were purchased from Sigma-Aldrich. All the solutions were prepared with ultrapure water (0.22 μS, 25 °C, Milli-Q®, Millipore).

This journal is © The Royal Society of Chemistry 2021

Environ. Sci.: Nano, 2021, 8, 3524–3535 | 3525

Synthesis and characterization of nano-MeJ

Amorphous calcium phosphate (ACP) nanoparticles were synthesized by a simple batch precipitation method at room temperature, following a protocol previously reported.[29] Briefly, two solutions, (A) $Ca(NO_3)_2$ (0.2 M) and Na_3Cit (0.2 M) and (B) K_2HPO_4 (0.12 M) and Na_2CO_3 (0.1 M), were mixed (1 : 1 v/v, 100 mL total) under agitation for 5 minutes. The precipitates were collected and repeatedly washed with ultrapure water by centrifugation (5000 rpm, 15 min, 18 °C). Afterwards, 200 mg of ACP nanoparticles were dispersed in 10 mL of ultrapure water with vigorous vortex and different amounts of MeJ were added to the nanoparticle suspension: 200 mg (nano-MeJ200), 40 mg (nano-MeJ40), 20 mg (nano-MeJ20) and 10 mg (nano-MeJ10). After 24 hours under agitation at room temperature, nano-MeJ was isolated from unbound MeJ by centrifugation (12 000 rpm, 15 min, 18 °C) and stored at 4 °C. Small quantities of sample were freeze-dried (Telstar) for further characterization. The MeJ concentration in solution was quantified by UV spectroscopy (Thermo Spectronic Unicam UV 300, USA) considering the strongest absorption band of the MeJ ketone group (λ = 291 nm, Section S1, Fig. S1, ESI†).[46] The loading capacity, *i.e.*, adsorbed MeJ (mg) per mg of nano-MeJ (% wt), was calculated by quantifying the MeJ delivered from a known amount of nano-MeJ after 3 days of delivery (when 100% release was achieved, Fig. 4). The MeJ adsorption efficiency (%) was calculated according to the following equation:

$$\text{Adsorption Efficiency (\%)}$$
$$= \frac{\text{Initial MeJ (mg)} - \text{non adsorbed MeJ (mg)}}{\text{Initial MeJ (mg)}} \cdot 100$$

where 'Initial MeJ' is the mass of MeJ added into the initial solution and 'non-adsorbed MeJ' is the mass of MeJ in the supernatant collected after the adsorption.

The Fourier transform infrared (FTIR) spectra of the nano-MeJ samples were recorded on a Tensor 27 (Bruker, Karlsruhe, Germany) spectrometer. Each powdered sample (2 mg) was mixed with 200 mg of anhydrous potassium bromide (KBr) and pressed at 5 tons into a 12 mm diameter disc using a hydraulic press (Specac). Three KBr pellets were produced for each sample, and a pure KBr disk was used as a blank. The infrared spectra were collected from 400 cm^{-1} to 4000 cm^{-1} at a resolution of 4 cm^{-1}. X-ray powder diffraction (XRPD) was performed on a Bruker D8 Advance diffractometer (from the Centre for Scientific Instrumentation of the University of Granada, CIC-UGR) using Cu Kα radiation (λ = 1.5406 Å), from 15° to 55° (2θ) with a scan rate of 40 s per step and a step size of 0.02° with a HV generator set at 50 kV and 1 mA. Transmission electron microscopy (TEM) analyses were performed with a LIBRA 120 PLUS instrument (Carl Zeiss SMT, CIC-UGR), operating at 120 kV. Nano-MeJ nanoparticles were ultrasonically dispersed in ethanol, and later, some drops of the slurry were deposited on 200 mesh copper grids covered with thin amorphous carbon films. The evaluation of the chemical composition (Ca, P and K) was performed by inductively coupled plasma optical emission spectrometry (ICP-OES, Optima 8300, PerkinElmer, CIC-UGR). Firstly, 2 ml of ultrapure nitric acid was used to dissolve 20 mg of the powdered sample. Secondly, the mix was diluted up to 100 mL with Milli-Q water. Three measurements of Ca, P and K contents were carried out each in triplicate. The corresponding emission wavelengths were 766.49 nm (K), 317.93 nm (Ca) and 213.62 nm (P). Nano-MeJ and the naked nanoparticles (control) were suspended in ultrapure water (0.5 mg mL^{-1}) containing 0.1% v/v of polyoxyethylene (20) sorbitan monooleate (Tween-80, Sigma-Aldrich) to measure the zeta potential with a Litesizer 500 (Anton Paar, Austria) through electrophoretic mobility.

Stability of nano-MeJ upon storage

Nano-MeJ was stored at 4 °C and its stability was evaluated after up to 12 months. At specific times, the sample was collected, freeze-dried and characterized by FTIR spectroscopy and X-ray diffraction. Calcium ions, dissolved during the storage, were quantified by ICP-OES following the protocol described above.

In vitro cytotoxicity assay

Human embryonic kidney (HEK293, ECACC 85120602) and mouse skin melanoma (B16-F10, ATCC CRL-6322) cell lines were purchased from the Cell Bank of CIC-UGR. HEK293 and B16-F10 were expanded in Eagle's minimum essential medium (EMEM) with Earle's balanced salt solution (EBSS) supplemented with 2 mM glutamine and 10% foetal bovine serum (FBS) at 37 °C in a humidified atmosphere of 5% CO$_2$. For HEK293 expansion, the cell medium was also supplemented with 1% nonessential amino acids (NEAA) and 1 mM sodium pyruvate (NaP).

The cells were detached from culture flasks by trypsinization, centrifuged and resuspended. The cell number and viability were assessed with the trypan-blue dye exclusion test. Then, 1.0×10^4 cells per well were seeded in a 96 flat transparent well and incubated at 37 °C in a humidified atmosphere of 5% CO$_2$. After 24 hours, different concentrations of MeJ, nano-MeJ and non-functionalized nanoparticles (nano-control) were added. The cells were exposed to equimolar amounts of MeJ, either free MeJ or coupled to nanoparticles (nano-MeJ): 0.25, 0.5, 1, 2, 3, 5, and 10 mM. The nano-control was tested at the same nanoparticle concentrations as nano-MeJ. After 2 days of incubation, the cell viability was evaluated by the MTS assay using CellTiter 96® AQueous One Solution Reagent (Promega, Madison, WI) according to the manufacturer's instructions. Briefly, 20 µL of AQueous One Solution Reagent was added to each well and after 2 h of incubation, the absorbance at 490 nm was measured with a spectrophotometer (Infinite® 200 PRO NanoQuant, CIC-UGR). The viability of parallel cultures of untreated cells was taken as 100% viability and the values obtained from the

3526 | *Environ. Sci.: Nano*, 2021, **8**, 3524–3535

This journal is © The Royal Society of Chemistry 2021

cells undergoing the different treatments (MeJ, nano-MeJ and nano-control) were referenced to this value. The half-maximal inhibitory concentration (IC_{50}), which indicates the concentration of compound required to inhibit cell growth at 50%, was calculated for MeJ and nano-MeJ with both cell lines. Each experiment was done in triplicate.

MeJ release kinetics in aqueous medium

The release kinetics of MeJ at room temperature was monitored by UV-vis spectroscopy (Cary 100, Agilent Technologies, Santa Clara, CA, USA). 40 mg of nano-MeJ was placed in a quartz cuvette and then, 2 mL of an aqueous solution of Tween-80 (0.1% v/v) was added. The absorbance at λ = 291 nm was measured in continuous mode until reaching a constant value (*i.e.*, plateau). The measurements were performed in triplicate.

In vivo field experiments on vineyards

The experiments were conducted in a randomized block design, in which five treatments were applied to three replicates, using 10 vines for each replication. Monastrell (*Vitis vinifera* L.) grapevines from experimental vineyards located in Cehegín (Murcia, Spain) were sprayed with five treatments as follows: aqueous solution of MeJ at concentrations of 5 mM and 10 mM (MeJ5 and MeJ10), aqueous suspension of 3.6 g L^{-1} ACP nanoparticles (nano-control), aqueous suspension of 3.6 g L^{-1} nano-MeJ (resulting in a total concentration of 1 mM MeJ) and aqueous solution of Tween-80 (0.1% v/v, control), which was used as a wetting and dispersant agent in all the treatments. 200 mL of the product was foliarly applied to each plant at grape veraison. A second application was performed after 7 days. The selection of the timing and dosage of the conventional treatments was based on previous results.[47–49] The MeJ concentration used in field experiments on vineyards to stimulate stilbene production was 10 mM.[49] On the basis of a previous study, in which the application of U-ACP (ACP nanoparticles loaded with urea) allowed a considerable reduction (15×) of nitrogen dosage while maintaining the quality parameters of Tempranillo grapes (in terms of amino acid content and yeast assimilable nitrogen),[42] we decided to apply ten times lower MeJ dosage (1 mM) with the nanoparticles.

Grapes were harvested at their optimum maturity, *i.e.* when the weight of 100 berries remained constant and the alcohol reached around 13% v v^{-1} (13° Braumé, Table S2†).[50] Vinification was carried out in triplicate in 50 L stainless steel tanks using 50 kg of grapes, which were destemmed, crushed, and sulfited (8 g SO_2/100 kg). The total acidity was corrected to 5.5 g L^{-1} with tartaric acid, and selected yeasts were added (Uvaferm VRB, Lallemand, 25 g h L^{-1}). The fermentative pomace contact period was 10 days during which the cap was punched down twice a day, and the temperature and must density were recorded. At the end of alcoholic fermentation, wines were pressed at 1.5 bar in a 75 L tank membrane and packed in bag-in-box for further analysis.

Stilbene analysis in wines

The extraction method used was described by Guerrero *et al.*[51] with some modifications. Briefly, 5 mL of wine was extracted with 5 mL of diethyl ether to which 25 μL of internal standard (*trans*-4-hydroxystilbene, 98%) was added. Samples were homogenized with an Ultraturrax T-25 (Jankel and Kunkel, IKA-Labortechnik, Germany) and stirred at 9600 rpm for 1 minute. The solutions were centrifuged (Eppendorf 5810-R centrifuge) at 10000 rpm for 10 minutes at 4 °C. The organic phase was dried in a CentriVap concentrator (CentriVap Labconco, USA) and the samples were diluted in 0.5 mL MeOH and filtered through a nylon 0.20 μm filter. During the extraction process, the samples were maintained in the dark and at low temperature to avoid possible oxidation and isomerization.

Stilbenes were identified and quantified by HPLC. Samples were analysed using a Waters2695 system equipped with a mass detector (Acquity QDA Waters). A 5 μm particle size 25 × 0.4 cm C-18 reversed phase column (LiChrospher 100 RP-18, Merck, Darmstadt, Germany) was used. The analysis was carried out at 25 °C and the injected sample volume was 10 μL. The separation was carried out in a gradient using formic acid (1%) and acetonitrile as mobile phases, with a flow of 1 mL min^{-1}. Mass spectrometry (MS) analyses were performed with an electrospray ionisation source (ESI) in negative mode with a sampling frequency of 5 points per s. The capillary and fragmentor potentials were set respectively to 0.8 kV and 40 V. The QDA analyser was operated in full scan mode, and the mass range was set at m/z 200–500. Stilbenes were quantified at 320 nm using *trans*-resveratrol, *trans*-piceid, piceatannol and ε-viniferin as external standards.

In vitro nano-MeJ protection assays

Solutions containing MeJ (10 mM) and nano-MeJ (with a total concentration of 2 mM) were placed on a glass slide in 100 μL drops to emulate the conditions in the field after spraying the leaves. Both of them were kept at 50 °C for 24 h. At scheduled times, the drops were observed using an iScope (Euromex) microscope with a 40× objective lens in bright field mode. After 24 hours, the remaining samples were analysed by Raman spectroscopy (JASCO NRS-5100, Jasco International Co. Ltd, Japan, CIC-UGR). The excitation line was provided by a diode laser emitting at a wavelength of 785 nm. The detector used was a Peltier cooled charge-couple device (CCD, 1024 × 256 pixels). Before the measurement, the Raman shift of the spectrometer was calibrated using the 520.7 cm^{-1} peak of crystalline silicon as the standard. Each spectrum corresponds to the average of 3 acquisitions of 100 s each. The spectra were linearly baseline corrected for clarity.
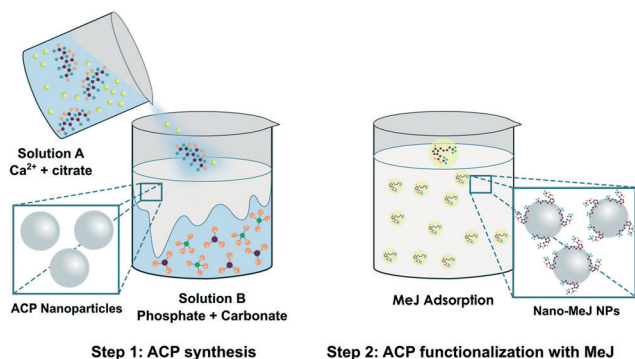
Scheme 1 Graphical sketch of the nano-MeJ preparation consisting of two-step process. ACP synthesis (Step 1) and MeJ adsorption on ACP (Step 2).

The same experiment was carried out by depositing on a crystallizer 20 drops of 100 μL of each sample to determine the ratio of protection. After 24 hours, MeJ drops were collected with 1 mL of water:ethanol (50:50) solution and the concentration of MeJ was measured by UV-vis spectroscopy (Fig. S1†). Then, the sample was centrifuged (12 000 rpm, 10 minutes) to remove the nanoparticles before UV-vis measurements. The ratio of protection (%) was calculated as $[MeJ]_{final}/[MeJ]_{initial} \times 100$. Each test was performed in triplicate.

Fresh vineyard leaves were treated with 100 μL of MeJ solutions (2 and 10 mM) and nano-MeJ (2 mM). Control leaf samples were treated with water. Images of the leaves were collected before and 24 hours after the treatments. The leaf treated with nano-MeJ was fixed with glutaraldehyde solution (2.5% in cacodylate buffer, 0.1 M, pH = 7.4) for 24 hours at 4 °C. Then, the sample was washed three times with cacodylate buffer and three times with ultrapure water. After that, the sample was dehydrated in a graded series of ethanol 50–70–90–100% (v/v), dried at the CO_2 critical point (Leica EM CPD300), mounted on metal stubs with conductive adhesive and covered with a thin carbon film. The sample was analysed using a field emission scanning electron microscope (GEMINI® FESEM, Carl Zeiss, CIC-UGR) operating at 5 kV.

Statistical analysis

Statistical comparisons were analysed with GraphPad Prism software (version 6.0) using one-way or two-way ANOVA and Bonferroni's *post hoc* test. When *P*-values are lower than 0.05 (*i.e.*, $P < 0.05$), differences in the obtained numerical results were considered statistically significant. IC_{50} values were calculated with the GraphPad Prism, using the dose–response sigmoidal curves ($P < 0.05$).

Results and discussion

Synthesis optimization and characterization of nano-MeJ

The experimental conditions were optimized with the aim of loading the maximum amount of MeJ on ACP nanoparticles (Scheme 1). To this aim, freshly prepared ACP nanoparticles (200 mg) were incubated with increasing quantities of MeJ: 10 mg (nano-MeJ10), 20 mg (nano-MeJ20), 40 mg (nano-MeJ40) and 200 mg (nano-MeJ200). The FTIR spectrum of nano-MeJ200 (Fig. 1a) shows typical phosphate absorption bands of ACP[52] along with a sharp peak at ~1740 cm^{-1} attributed to carbonyl (ketone) groups of MeJ (Fig. S2†).[53] The XRD pattern of this sample exhibits two broad bands: one at 30° (2θ) characteristic of ACP and the other at 20° (2θ), due to the diffuse scattering of non-adsorbed MeJ (Fig. 1b, nano-MeJ200). The latter feature was not observed in the XRD patterns of nano-MeJ synthesized with lower MeJ concentrations (Fig. 1b), revealing the formation of ACP–MeJ nanocomposites. However, nano-MeJ10 contained very low concentration of MeJ since the band at 1740 cm^{-1} was practically negligible (Fig. 1a). On the basis of the XRD and FTIR results, nano-MeJ20 and nano-MeJ40 composites were selected as the most suitable conditions for further analyses.

We evaluated the MeJ loading capacity (%) and adsorption efficiency (%) by UV-vis spectroscopy (ESI† S1). Nano-MeJ20 and nano-MeJ40 contained similar contents of MeJ (6.2 ± 1.7% and 4.7 ± 1.1%, respectively). This means that the adsorption on ACP reached a plateau when adding 20 mg and thus doubling MeJ did not modify the loading. Consequently, the adsorption efficiency was much higher for
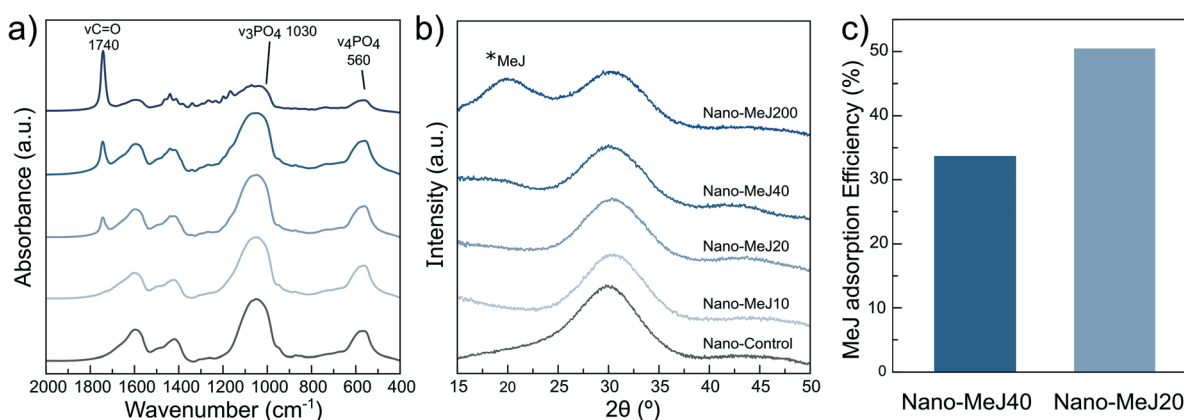

Fig. 1 (a) FTIR spectra and (b) XRD patterns of ACP nanoparticles (nano-Control) and nano-MeJ synthesized with increasing MeJ concentrations (nano-MeJ10, nano-MeJ20, nano-MeJ40 and nano-MeJ200). (c) MeJ adsorption efficiency for nano-MeJ40 and nano-MeJ20.

3528 | *Environ. Sci.: Nano*, 2021, **8**, 3524–3535

This journal is © The Royal Society of Chemistry 2021

nano-MeJ20 (Fig. 1c). Hence, nano-MeJ20 was selected as the optimal nanocomposite material and hereafter is referred to as nano-MeJ. After the adsorption, the concentration of non-adsorbed MeJ in the supernatant was directly measured by UV-vis (ESI,† S1). The remaining solution containing non-adsorbed MeJ was used in successive adsorption experiments, thus maintaining the whole synthetic process environmentally sustainable and efficient. This is highly relevant when considering the high costs of MeJ and its associated cytoxicity.[54]

The compositional analysis of nano-MeJ by ICP-OES indicated a Ca/P molar ratio close to 1.5 (Table S1†), which is characteristic of ACP.[55] The MeJ adsorption therefore did not affect the ACP composition. The morphology was neither affected by MeJ adsorption (Fig. S3†).[29] The ζ-potential of the nano-control and nano-MeJ was, respectively, −15.7 ± 0.6 mV and −10.3 ± 0.7 mV (Table S1†). The increase in ζ-potential (less negative) can be associated with MeJ adsorption on the ACP surface.

Stability of nano-MeJ upon storage

The long-term stability of nano-MeJ stored at 4 °C was monitored by FTIR spectroscopy and X-ray diffraction (Fig. 2 and S4†). The FTIR spectrum collected after 49 days showed the sharpening of the main phosphate vibrational bands (500–600 and 900–1100 cm^{-1}), suggesting that ACP evolved to poorly crystalline apatite (Fig. 2a). Two broad Bragg peaks at around 26° and 32° (2θ) emerged in the XRD pattern of the same sample (Fig. S4†), confirming the conversion. It is well-known that ACP is a transient precursor that converts into the thermodynamically stable phase (apatite or octacalcium phosphate, depending on the experimental conditions).[56]

Calcium ions in solution were also measured by ICP-OES as an indicator of the chemical stability of the nanoparticles upon storage. Less than 2% (w/w) of the total calcium was dissolved after 49 days. Concomitantly with the ACP-to-Ap conversion and the practically negligible nanoparticle dissolution, we found a slight decrease in the intensity of the MeJ absorption band after 49 days of storage (Fig. 2b). This effect is associated with the partial desorption of MeJ, occurring when ACP transforms into Ap.[57] Indeed, ACP is endowed with higher capacity to host exogenous ions or molecules (e.g. citrate, urea, MeJ) than apatite nanocrystals.[29,55,57] Despite the slight decrease of the MeJ band after 49 days, it remained constant up to 175 days confirming the long-term chemical stability of nano-MeJ. This aspect is very important for the real application of the product.

In vitro cytotoxicity of nano-MeJ

The application of nano-agrochemicals may raise concern about nanomaterial safety along the whole life-cycle, including production, storage and transport, handling by farmers and possible accumulation in the food chain.[58] Here, we have evaluated the cytotoxicity of MeJ and nano-MeJ
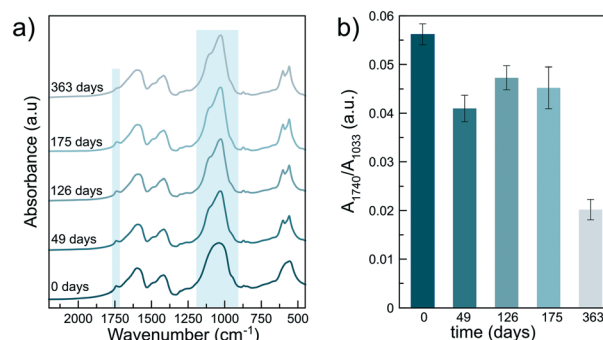

Fig. 2 Long-term stability of nano-MeJ upon storage. (a) FTIR spectra of the nano-MeJ sample stored at 4 °C for up to 0, 49, 126, 175 and 363 days. The spectra were normalized by the maximum intensity (at *ca.* 1030 cm^{-1}) and vertically offset for the sake of clarity. (b) Area ratio of the bands associated with MeJ and calcium phosphate (A_{1740}/A_{1033}) as a function of storage time (days). The intervals used to estimate the area are highlighted in (a).

against B16-F10 and HEK-293 cell lines by the MTS assay. Fig. 3 shows the cell viability expressed as a percentage with respect to untreated control cells. Free MeJ showed higher cytotoxicity than nano-MeJ ($p < 0.001$) for both cell lines (Fig. 3). In the case of melanoma cells, the IC_{50} value of free MeJ was 2.2 mM whereas this value increased up to 4.7 mM for nano-MeJ, indicating its lower associated toxicity. The IC_{50} value of free MeJ is in agreement with previous reports showing that 2.6 mM MeJ was needed to decrease by half the cell viability of the same cell line.[59] HEK-293 also showed a higher IC_{50} value for nano-MeJ than for free MeJ, being 3.8 and 2.9 mM, respectively. The lower toxicity of MeJ coupled to ACP nanoparticles is remarkably advantageous for the safe handling and use of MeJ in agriculture. Conversely, ACP nanoparticles (Fig. 3, nano-control) affected neither the B16-F10 nor the HEK293 cell viability at the tested concentrations, as was already observed in previous studies.[29]

Release kinetics in aqueous media

The delivery of MeJ from nanoparticles in the presence of Tween-80 was monitored by UV-vis for several days. The time-dependent profile is shown in Fig. 4. It follows a gradual and slow release for 50 hours, reaching then a steady state (plateau). The experimental data were fitted to a first-order release model, resulting in a good fit for a release rate of $k = 0.05$ h^{-1} ($R^2 = 0.97$, inset of Fig. 4). The release rate (and profile) was very similar to that obtained in ultrapure water ($k = 0.045$ h^{-1}, Fig. S5†), so the presence of Tween-80 did not affect the MeJ delivery. The low solubility of MeJ in water (340 mg L^{-1}) may explain such a slow release profile, comparable to that observed for a poor water-soluble drug such as doxorubicin from apatite nanoparticles.[60] In fact, the release rate is much slower than that observed for water-soluble species adsorbed on the ACP surface, such as urea and nitrate ($k(N) = 1.97$ h^{-1}).[29] The MeJ desorption rate is

This journal is © The Royal Society of Chemistry 2021

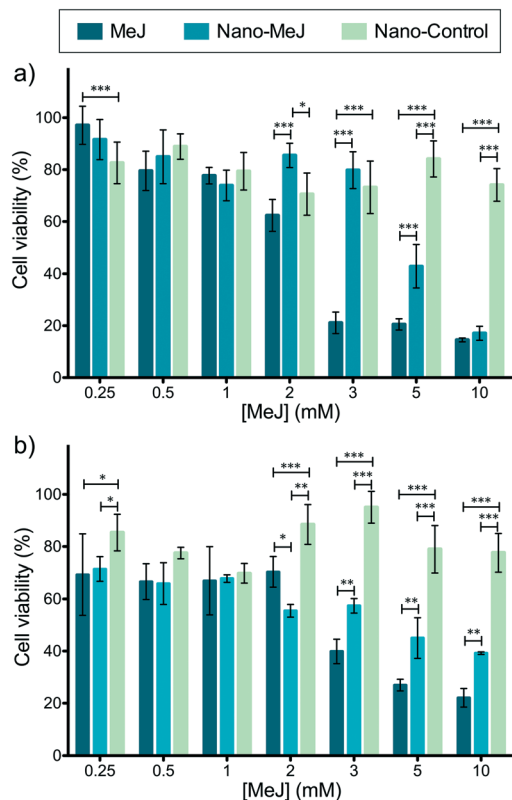*Environ. Sci.: Nano*, 2021, **8**, 3524–3535 | **3529**

Fig. 3 Effects of MeJ, nano-MeJ and ACP nanoparticles (nano-control) on the B16-F10 (a) and HEK293 (b) cell viability. The relative cell viability (%) corresponds to the absorbance ratio between treated and non-treated cells (*i.e.*, [A]sample/[A]control × 100). Data are expressed as mean with their corresponding standard deviation as error bars. Statistically significant differences between treatments are marked with * (*P*-value < 0.05) or *** (*P*-value < 0.001).

similar to that of nanoparticle dissolution in water (0.02 h^{-1} < k < 0.03 h^{-1}),[29] which indicates that MeJ is delivered upon
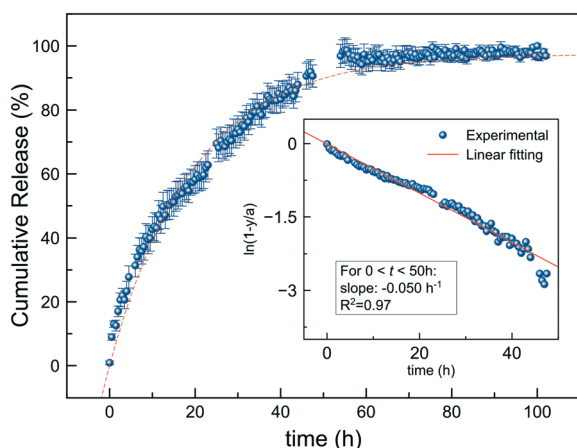

Fig. 4 MeJ release profile from nano-MeJ in aqueous solution containing 0.1% v/v of Tween-80. The dashed line represents the best fits of the experimental data to the first order equation: $y(t) = a \times (1 - e^{-kt})$, with the rate constant $k = 0.05$ h^{-1}. The inset shows the linearized experimental data (symbols) and the first order equation (line).

partial dissolution of the nanoparticles, following thus a similar release profile.

In vivo field experiments on Monastrell vineyards

Recent *in vitro* experiments on *V. vinifera* cell cultures have shown that the application of MeJ encapsulated in poly(lactic-*co*-glycolic acid) nanoparticles (PLGA NPs) provided an important enhancement of stilbene production in comparison to the application of free MeJ.[22] Very low concentrations of MeJ (25 μM) were needed to observe important effects when comparing between treatments.[22] Indeed, cells treated with MeJ-loaded PLGA NPs showed an increase of total stilbenes of about 11 times compared to the control and almost triple than free MeJ-treated cells. However, extrapolating these interesting effects to more complex scenarios such as field treatments in grapevines requires the application of a much higher MeJ dosage. Increasing the stilbene composition in wines is even more challenging. In fact, previous field experiments confirmed that the foliar application of 10 mM MeJ was needed to promote stilbene production in grapes and wines.[7,12]

We have explored the possibility of reducing the MeJ dosage with the nano-MeJ application. During the veraison, the leaves of the Monastrell grapevines were sprayed with aqueous solutions of nano-MeJ (1 mM). For the sake of comparison, leaves of different grapevines were sprayed with aqueous solutions of 5 or 10 mM MeJ (MeJ5 or MeJ10). Grapes treated with MeJ10 resulted in wines with a significant (p < 0.001) increase of the total stilbene concentration with respect to non-treated grapes (control, Fig. 5a). Surprisingly, the application of nano-MeJ, with a ten-fold reduction of dosage, produced a similar level of stilbene in wines (Fig. 5a). Noteworthily, the application of MeJ5 was not enough to produce the same enhancement in stilbene concentration (MeJ5, Fig. 5a), confirming 10 mM as the minimum concentration to observe important effects when the elicitor is conventionally applied. Similar positive effects were previously observed after the foliar application of urea-doped ACP (U-ACP) nanoparticles to Tempranillo grapevines, which produced musts with a significant increase of amino acid concentration and yeast assimilable nitrogen, similar to those obtained with conventional treatments (crystalline urea) containing 15 times higher urea concentrations.[42]

The concentration of stilbene phenolic compounds in grapes and wines depends on multiple factors including the intrinsic properties of grape variety, climate, growth conditions, harvest year and enological procedures.[12] In fact, Monastrell grapes are considered as a high resveratrol producer.[12] In this study, *trans*-resveratrol was the major stilbene found in wine, comprising around the 90% of the total stilbenes (Fig. 5a and b). All the MeJ-based treatments increased the concentration of *trans*-resveratrol in wine with respect to the controls (Fig. 5b). The *cis*-resveratrol isomer has received much less attention, probably due to its very low concentration in grapes and wine. Our results indicated that
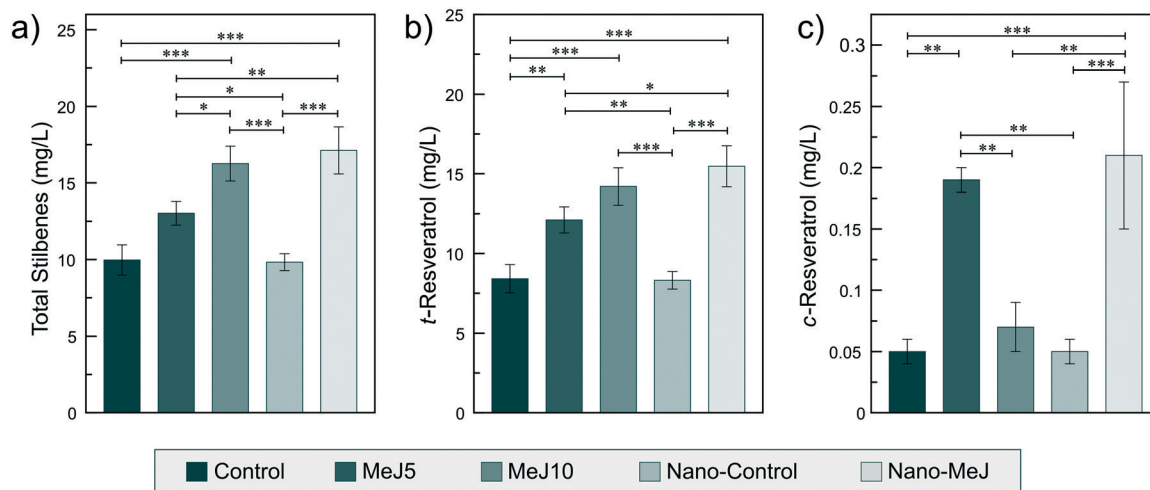
3530 | *Environ. Sci.: Nano*, 2021, **8**, 3524–3535

This journal is © The Royal Society of Chemistry 2021

Fig. 5 Concentration (mg L^{-1}) of total stilbenes (a), *trans*-resveratrol (b) and *cis*-resveratrol (c) in wines from grapes treated with water solutions containing 5 mM (MeJ5) and 10 mM (MeJ10) MeJ and 1 mM nano-MeJ. Results of grapes treated with naked nanoparticles (nano-control) and non-treated grapes (control) are also shown. Data are expressed as mean with their corresponding standard deviation as error bars. Statistically significant differences between measurements are marked with * (P-value < 0.05), ** (P-value < 0.01) or *** (P-value < 0.001).

only the treatments MeJ5 and nano-MeJ produced a significant increase with respect to the controls (Fig. 5c). A possible explanation is that high concentrations of MeJ (10 mM) hinder the production of the *cis*-isomer. However, further studies are needed to confirm this assumption. Regarding other important stilbenes, nano-MeJ increased the *cis*- and *trans*-piceid concentrations in wine, to the same extent as conventional MeJ treatments (Fig. S6†). From the comparison of the control and the nano-control treatments (Fig. 5 and S6†), we can also conclude that naked nanocarriers do not stimulate the plants to induce the production of stilbene.

In vitro study of MeJ and nano-MeJ evolution in droplets: protection and retention

With the aim of explaining the interesting *in vivo* results, we studied the evolution of MeJ and nano-MeJ in aqueous droplets simulating the conditions occurring in the fields after spraying the leaves. The evolution of the drops deposited on glass covers was monitored by optical microscopy. Micron-sized micelles were found under the microscope soon after the deposition of the drops containing 10 mM MeJ (Fig. 6a, top, t_0). These drops were completely dried after a few hours at 50 °C, leaving a holey microstructure with an oily appearance that did not change after 24 hours (Fig. 6a, top). Raman micro-analysis on different zones of this microstructure (Fig. S7†) did not show signals assignable to MeJ, suggesting that MeJ was evaporated after 24 hours. To confirm this hypothesis, the experiment was repeated with 20 droplets (100 μL each) of a 10 mM MeJ solution. The remaining MeJ concentration after 24 hours at 50 °C was quantified by UV-vis spectroscopy. Only a small percentage (11%) remained on the glass surface (Fig. 6b), confirming the previous observations.

Conversely, drops of nano-MeJ contained floating microparticles as the result of nanoparticle aggregation but micelles of MeJ were not found (Fig. 6a, bottom, t_0). The drops were completely dried after 3 hours and 30 minutes at 50 °C and the nano-MeJ aggregates settled on the glass surface (Fig. 6a, bottom). Raman micro-analysis of the mineral aggregates, which remained unaltered for several days at 50 °C, confirmed the presence of MeJ (Fig. S7†). Indeed, UV-vis quantification indicated that 90% of initial MeJ remained on the glass after 24 hours at 50 °C (Fig. 6b).

A similar behaviour was observed on the surface of the grapevine leaves during the treatments in the field (Fig. 7). Photographs of the leaves collected several hours after being sprayed with nano-MeJ showed white spots of mineral deposits, which were not observed on the leaves treated with MeJ solutions (Fig. 7a). A closer look at the surface of the leaves by FESEM revealed that the micron-sized mineral aggregates were composed of nanoparticles with the typical (round-shaped) morphology of ACP (Fig. 7b). We observed the appearance of necrotic lesions on the leaves treated with
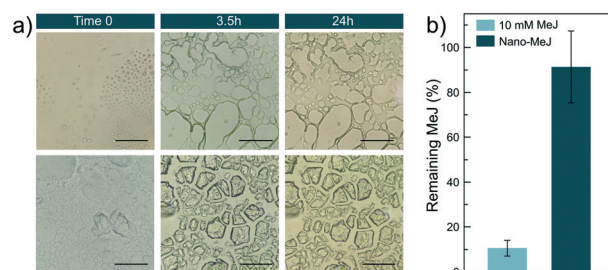

Fig. 6 (a) Optical micrographs of drops containing MeJ (top) and nano-MeJ (bottom) collected at different time intervals at 50 °C. Scale bar = 100 μm. (b) Percentage of remaining MeJ (quantified by UV-vis spectroscopy) after 24 hours at 50 °C for both treatments.
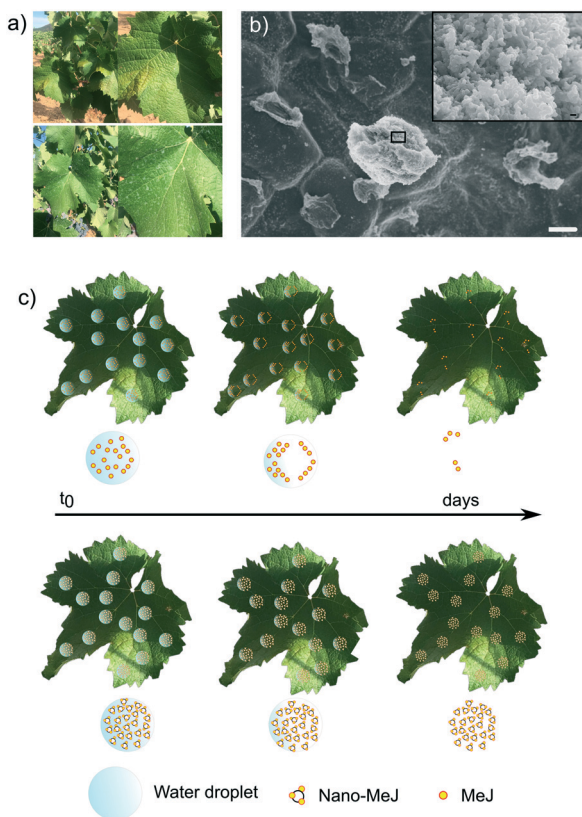
This journal is © The Royal Society of Chemistry 2021

Environ. Sci.: Nano, 2021, **8**, 3524–3535 | **3531**

Paper

Environmental Science: Nano

Fig. 7 (a) Pictures of vineyard leaves treated with 10 mM MeJ (top) and nano-MeJ (bottom). (b) FESEM micrograph of the leaf surface showing nano-MeJ aggregates. Scale bar = 100 μm. The inset shows details of the nanostructure (round-shaped nanoparticles) of the aggregates. Scale bar = 200 nm. (c) Graphical sketch of the evolution of MeJ and nano-MeJ in the aqueous droplets after spraying the leaves.

2 or 10 mM MeJ, not found on the leaves treated with nano-MeJ (Fig. S8†). Previous studies reported highly phytotoxic effects associated with high MeJ concentrations.[21,61] MeJ concentrations ranging from 5 to 20 mM caused the propagation of necrotic lesions on cucumber leaves, whereas acute MeJ concentrations (50 mM) led to the activation of programmed cell death and subsequent rapid propagation of necrosis over the entire leaf surface.[61] In our *in vivo* experiments, normal values of enological quality parameters of the musts (pH, acidity and degree Braumé, Table S2†) were found and practically unaffected for all the treatments. Thus, we did not find further evidence of phytotoxicity under the explored conditions, despite the leaf damage caused by the conventional treatments (Fig. S8†).

On the basis of the above experimental results, we propose the mechanism of protection and retention of the elicitor as depicted in Fig. 7c. After spraying the MeJ-containing solution (5 mM or 10 mM) on the leaves, the solvent (water) and MeJ evaporated in a few hours, losing *ca.* 90% of the elicitor in 24 hours (Fig. 7c, top). In contrast, the application of nano-MeJ ended up with the precipitation of nanostructured aggregates on the surface of the leaves, which

retained the elicitor (Fig. 7c, bottom). Indeed, 90% of the elicitor remained on the glass surface in contact with nano-MeJ drops after 24 hours (Fig. 6b). This boosts the prolonged and sustained supply of the elicitor through the leaves, causing the efficiency increase observed with the nano-MeJ treatments in the *in vivo* field experiments. Unfortunately, our experimental results do not provide information on the absorption mechanisms, being the plant still a black box. Further experiments dedicated to track the fate of the nanoparticles inside the plants are needed to progress in this direction.

Conclusions

A novel nanocomposite to be used as an elicitor able to trigger plant defence responses in plants was developed here. ACP nanoparticles were efficiently functionalized with MeJ, an elicitor with important implications in plant physiology and growth. We optimized the synthetic conditions to achieve a loading efficiency of 50% and a payload of *ca.* 6 wt% of MeJ. This novel organic/inorganic nanocomposite showed long-term stability (175 days at 4 °C) and lower cytotoxicity compared to free MeJ, facilitating safer handling and application of the resistance-inductor elicitor. The efficiency of the nanoparticles in delivering the elicitor was assayed *in vivo* by means of field experiments on Monastrell vineyards. Wines from grapes of plants treated with nano-MeJ gave rise to a significant increase in total stilbenes, similar to the content obtained with a conventional treatment but with 10 times higher MeJ concentration. *In vitro* protection assays revealed that the nanoparticles hindered MeJ evaporation and/or thermal degradation. This protection effect along with the gradual release may ensure MeJ activity over longer periods of time. This results in a considerable reduction of MeJ dosage while maintaining the quality of the harvest, thereby mitigating the compelling environmental impact derived therefrom.

Author contributions

Conceptualization: J. M. D.-L., R. G.-M. and G. B. R.-R.; investigation: B. P.-T., M. J. G.-B., J. D. M.-O. and D. F. P.-Q.; funding acquisition and supervision: J. M. D.-L. and R. G.-M.; writing – original draft: J. M. D.-L. and G. B. R.-R.; writing – review and editing: all the authors. All authors have read and agreed to the published version of the manuscript.

Conflicts of interest

There are no conflicts to declare.

Acknowledgements

Notes and references

1 S. Kumar, M. Nehra, N. Dilbaghi, G. Marrazza, A. A. Hassan and K.-H. Kim, Nano-based smart pesticide formulations: Emerging opportunities for agriculture, *J. Controlled Release*, 2019, **294**, 131–153.

2 H.-R. Köhler and R. Triebskorn, Wildlife Ecotoxicology of Pesticides: Can We Track Effects to the Population Level and Beyond?, *Science*, 2013, **341**, 759–765.

3 N. Benhamou, Elicitor-induced plant defence pathways, *Trends Plant Sci.*, 1996, **1**, 233–240.

4 H. Gundlach, M. J. Müller, T. M. Kutchan and M. H. Zenk, Jasmonic acid is a signal transducer in elicitor-induced plant cell cultures, *Proc. Natl. Acad. Sci. U. S. A.*, 1992, **89**, 2389–2393.

5 J.-J. Cheong and Y. Do Choi, Methyl jasmonate as a vital substance in plants, *Trends Genet.*, 2003, **19**, 409–413.

6 H. Huang, B. Liu, L. Liu and S. Song, Jasmonate action in plant growth and development, *J. Exp. Bot.*, 2017, **68**, 1349–1359.

7 Y. Ruiz-Garcia, I. Romero-Cascales, R. Gil-Munoz, J. I. Fernandez-Fernandez, J. M. Lopez-Roca and E. Gomez-Plaza, Improving grape phenolic content and wine chromatic characteristics through the use of two different elicitors: Methyl jasmonate versus benzothiadiazole, *J. Agric. Food Chem.*, 2012, **60**, 1283–1290.

8 H. Yao and S. Tian, Effects of pre-and post-harvest application of salicylic acid or methyl jasmonate on inducing disease resistance of sweet cherry fruit in storage, *Postharvest Biol. Technol.*, 2005, **35**, 253–262.

9 H. J. Yao and S. P. Tian, Effects of a biocontrol agent and methyl jasmonate on postharvest diseases of peach fruit and the possible mechanisms involved, *J. Appl. Microbiol.*, 2005, **98**, 941–950.

10 C.-K. Ding, C. Y. Wang, K. C. Gross and D. L. Smith, Reduction of chilling injury and transcript accumulation of heat shock proteins in tomato fruit by methyl jasmonate and methyl salicylate, *Plant Sci.*, 2001, **161**, 1153–1159.

11 G. A. González-Aguilar, J. Fortiz, R. Cruz, R. Baez and C. Y. Wang, Methyl jasmonate reduces chilling injury and maintains postharvest quality of mango fruit, *J. Agric. Food Chem.*, 2000, **48**, 515–519.

12 R. Gil-Muñoz, J. I. Fernández-Fernández, O. Crespo-Villegas and T. Garde-Cerdán, Elicitors used as a tool to increase stilbenes in grapes and wines, *Food Res. Int.*, 2017, **98**, 34–39.

13 J. Portu, P. Santamaría, I. Lopez-Alfaro, R. Lopez and T. Garde-Cerdán, Methyl jasmonate foliar application to Tempranillo vineyard improved grape and wine phenolic content, *J. Agric. Food Chem.*, 2015, **63**, 2328–2337.

14 J. Portu, R. López, E. Baroja, P. Santamaría and T. Garde-Cerdán, Improvement of grape and wine phenolic content by foliar application to grapevine of three different elicitors: Methyl jasmonate, chitosan, and yeast extract, *Food Chem.*, 2016, **201**, 213–221.

15 S. Vezzulli, S. Civardi, F. Ferrari and L. Bavaresco, Methyl jasmonate treatment as a trigger of resveratrol synthesis in cultivated grapevine, *Am. J. Enol. Vitic.*, 2007, **58**, 530–533.

16 A. A. A. Bertelli and D. K. Das, Grapes, wines, resveratrol, and heart health, *J. Cardiovasc. Pharmacol.*, 2009, **54**, 468–476.

17 R. F. Guerrero, M. C. Garcia-Parrilla, B. Puertas and E. Cantos-Villar, Wine, resveratrol and health: a review, *Nat. Prod. Commun.*, 2009, **4**, 635–658.

18 M. Jang, L. Cai, G. O. Udeani, K. V. Slowing, C. F. Thomas, C. W. W. Beecher, H. H. S. Fong, N. R. Farnsworth, A. D. Kinghorn and R. G. Mehta, Cancer chemopreventive activity of resveratrol, a natural product derived from grapes, *Science*, 1997, **275**, 218–220.

19 J. A. Baur, K. J. Pearson, N. L. Price, H. A. Jamieson, C. Lerin, A. Kalra, V. V. Prabhu, J. S. Allard, G. Lopez-Lluch and K. Lewis, Resveratrol improves health and survival of mice on a high-calorie diet, *Nature*, 2006, **444**, 337–342.

20 Y. Ruiz-García, I. Romero-Cascales, A. B. Bautista-Ortín, R. Gil-Muñoz, A. Martínez-Cutillas and E. Gómez-Plaza, Increasing Bioactive Phenolic Compounds in Grapes: Response of Six Monastrell Grape Clones to Benzothiadiazole and Methyl Jasmonate Treatments, *Am. J. Enol. Vitic.*, 2013, **64**, 459–465.

21 U. Hartmond, R. Yuan, J. K. Burns, A. Grant and W. J. Kender, Citrus fruit abscission induced by methyl-jasmonate, *J. Am. Soc. Hortic. Sci.*, 2000, **125**, 547–552.

22 L. Chronopoulou, L. Donati, M. Bramosanti, R. Rosciani, C. Palocci, G. Pasqua and A. Valletta, Microfluidic synthesis of methyl jasmonate-loaded PLGA nanocarriers as a new strategy to improve natural defenses in Vitis vinifera, *Sci. Rep.*, 2019, **9**, 1–9.

23 P. Wang, E. Lombi, F.-J. Zhao and P. M. Kopittke, Nanotechnology: A New Opportunity in Plant Sciences, *Trends Plant Sci.*, 2016, **21**, 699–712.

24 S. Yan, Q. Hu, J. Li, Z. Chao, C. Cai, M. Yin, X. Du and J. Shen, A star polycation acts as a drug nanocarrier to improve the toxicity and persistence of botanical pesticides, *ACS Sustainable Chem. Eng.*, 2019, **7**, 17406–17413.

25 X. Wang, K. Zheng, W. Cheng, J. Li, X. Liang, J. Shen, D. Dou, M. Yin and S. Yan, Field application of star polymer-delivered chitosan to amplify plant defense against potato late blight, *Chem. Eng. J.*, 2021, **417**, 129327.

26 S. Ruffo Roberto, K. Youssef, A. F. Hashim and A. Ippolito, Nanomaterials as alternative control means against postharvest diseases in fruit crops, *Nanomaterials*, 2019, **9**, 1752.

27 M. Epple, Review of potential health risks associated with nanoscopic calcium phosphate, *Acta Biomater.*, 2018, **77**, 1–14.

28 J. Gómez-Morales, M. Iafisco, J. M. Delgado-López, S. Sarda and C. Drouet, Progress on the preparation of nanocrystalline apatites and surface characterization:

This journal is © The Royal Society of Chemistry 2021

Environ. Sci.: Nano, 2021, **8**, 3524–3535 | **3533**

Overview of fundamental and applied aspects, *Prog. Cryst. Growth Charact. Mater.*, 2013, **59**, 1–46.

29 G. B. Ramírez-Rodríguez, G. Dal Sasso, F. J. Carmona, C. Miguel-Rojas, A. Pérez-de-luque, N. Masciocchi, A. Guagliardi and J. M. Delgado-López, Engineering Biomimetic Calcium Phosphate Nanoparticles: A Green Synthesis of Slow-Release Multinutrient (NPK) Nanofertilizers, *ACS Appl. Bio Mater.*, 2020, **3**, 1344–1353.

30 F. J. Carmona, G. Dal Sasso, F. Bertolotti, G. B. Ramírez-Rodríguez, J. M. Delgado-López, J. S. Pedersen, N. Masciocchi and A. Guagliardi, The role of nanoparticle structure and morphology in the dissolution kinetics and nutrient release of nitrate-doped calcium phosphate nanofertilizers, *Sci. Rep.*, 2020, **10**, 1–13.

31 S. V. Dorozhkin and M. Epple, Biological and medical significance of calcium phosphates, *Angew. Chem., Int. Ed.*, 2002, **41**, 3130–3146.

32 R. L. Ruiqiang Liu, Synthetic apatite nanoparticles as a phosphorus fertilizer for soybean (Glycine max), *Sci. Rep.*, 2014, **4**, 5686.

33 L. Xiong, P. Wang, M. N. Hunter and P. M. Kopittke, Bioavailability and movement of hydroxyapatite nanoparticles (HA-NPs) applied as a phosphorus fertiliser in soils, *Environ. Sci.: Nano*, 2018, **5**, 2888–2898.

34 L. Marchiol, A. Filippi, A. Adamiano, L. Degli Esposti, M. Iafisco, A. Mattiello, E. Petrussa and E. Braidot, Influence of Hydroxyapatite Nanoparticles on Germination and Plant Metabolism of Tomato (Solanum lycopersicum L.): Preliminary Evidence, *Agronomy*, 2019, **9**, 161.

35 S. Tang and X. Fei, Refractory Calcium Phosphate-Derived Phosphorus Fertilizer Based on Hydroxyapatite Nanoparticles for Nutrient Delivery, *ACS Appl. Nano Mater.*, 2021, **4**, 1364–1376.

36 M. R. Maghsoodi, L. Ghodszad and B. Asgari Lajayer, Dilemma of hydroxyapatite nanoparticles as phosphorus fertilizer: Potentials, challenges and effects on plants, *Environ. Technol. Innovation*, 2020, **19**, 100869.

37 N. H. Madanayake, N. M. Adassooriya and N. Salim, The effect of hydroxyapatite nanoparticles on Raphanus sativus with respect to seedling growth and two plant metabolites, *Environ. Nanotechnol. Monit. Manag.*, 2021, **15**, 100404.

38 A. E. Szameitat, A. Sharma, F. Minutello, A. Pinna, M. Er-Rafik, T. H. Hansen, D. P. Persson, B. Andersen and S. Husted, Unravelling the interactions between nano-hydroxyapatite and the roots of phosphorus deficient barley plants, *Environ. Sci.: Nano*, 2021, **8**, 444–459.

39 A. S. Giroto, G. G. F. Guimarães, M. Foschini and C. Ribeiro, Role of slow-release nanocomposite fertilizers on nitrogen and phosphate availability in soil, *Sci. Rep.*, 2017, **7**, 46032.

40 N. Kottegoda, C. Sandaruwan, G. Priyadarshana, A. Siriwardhana, U. A. Rathnayake, D. M. Berugoda Arachchige, A. R. Kumarasinghe, D. Dahanayake, V. Karunaratne and G. A. J. Amaratunga, Urea-hydroxyapatite nanohybrids for slow release of nitrogen, *ACS Nano*, 2017, **11**, 1214–1221.

41 G. B. Ramírez-Rodríguez, C. Miguel-Rojas, G. S. Montanha, F. J. Carmona, G. Dal Sasso, J. C. Sillero, J. S. Pedersen, N. Masciocchi, A. Guagliardi, A. Pérez-De-luque and J. M. Delgado-López, Reducing nitrogen dosage in triticum durum plants with urea-doped nanofertilizers, *Nanomaterials*, 2020, **10**, 1–16.

42 E. P. Pérez-Álvarez, G. B. Ramírez-Rodríguez, F. J. Carmona, J. M. Martínez-Vidaurre, N. Masciocchi, A. Guagliardi, T. Garde-Cerdán and J. M. Delgado-López, Towards a more sustainable viticulture: foliar application of N-doped calcium phosphate nanoparticles on Tempranillo grapes, *J. Sci. Food Agric.*, 2021, **101**, 1307–1313.

43 H. Y. Yoon, J. G. Lee, L. D. Esposti, M. Iafisco, P. J. Kim, S. G. Shin, J.-R. Jeon and A. Adamiano, Synergistic Release of Crop Nutrients and Stimulants from Hydroxyapatite Nanoparticles Functionalized with Humic Substances: Toward a Multifunctional Nanofertilizer, *ACS Omega*, 2020, **5**, 6598–6610.

44 F. Carella, M. Seck, L. D. Esposti, H. Diadiou, A. Maienza, S. Baronti, P. Vignaroli, F. P. Vaccari, M. Iafisco and A. Adamiano, Thermal conversion of fish bones into fertilizers and biostimulants for plant growth-A low tech valorization process for the development of circular economy in least developed countries, *J. Environ. Chem. Eng.*, 2021, **9**, 104815.

45 A. Adamiano, G. Fellet, M. Vuerich, D. Scarpin, F. Carella, C. Piccirillo, J. R. Jeon, A. Pizzutti, L. Marchiol and M. Iafisco, Calcium phosphate particles coated with humic substances: A potential plant biostimulant from circular economy, *Molecules*, 2021, **26**, 1–15.

46 J. Islam, S. Phukan and P. Chattopadhyay, Development of a validated RP-HPLC/DAD method for the quantitative determination of methyl jasmonate in an insect repellent semi-solid formulation, *Heliyon*, 2019, **5**, e01775.

47 R. Gil-Muñoz, J. I. Fernández-Fernández, J. Portu and T. Garde-Cerdán, Methyl jasmonate: Effect on proanthocyanidin content in Monastrell and Tempranillo grapes and wines, *Eur. Food Res. Technol.*, 2018, **244**, 611–621.

48 R. Gil-Munoz, J. I. Fernandez-Fernandez, O. Crespo-Villegas and T. Garde-Cerdan, Elicitors used as a tool to increase stilbenes in grapes and wines, *Food Res. Int.*, 2017, **98**, 34–39.

49 G. Gutiérrez-Gamboa, R. Mateluna-Cuadra, I. Díaz-Gálvez, N. Mejía and N. Verdugo-Vásquez, Methyl Jasmonate Applications in Viticulture: A Tool to Increase the Content of Flavonoids and Stilbenes in Grapes and Wines, *Horticulturae*, 2021, **7**, 133.

50 T. Garde-Cerdán, G. Gutiérrez-Gamboa, E. Baroja, P. Rubio-Bretón and E. P. Pérez-Álvarez, Influence of methyl jasmonate foliar application to vineyard on grape volatile composition over three consecutive vintages, *Food Res. Int.*, 2018, **112**, 274–283.

51 R. F. Guerrero, B. Puertas, M. I. Fernández, M. Palma and E. Cantos-Villar, Induction of stilbenes in grapes by UV-C: Comparison of different subspecies of Vitis, *Innovative Food Sci. Emerging Technol.*, 2010, **11**, 231–238.

52 J. M. Delgado-López, M. Iafisco, I. Rodríguez, A. Tampieri, M. Prat and J. Gómez-Morales, Crystallization of bioinspired

3534 | *Environ. Sci.: Nano*, 2021, **8**, 3524–3535

This journal is © The Royal Society of Chemistry 2021

citrate-functionalized nanoapatite with tailored carbonate content, *Acta Biomater.*, 2012, **8**, 3491–3499.

53 T. Sato, T. Kawara, K. Sakata and T. Fujisawa, Jasmonoid Synthesis from sci-4-Heptenoic Acid, *Bull. Chem. Soc. Jpn.*, 1981, **54**, 505–508.

54 N. Goldin, L. Arzoine, A. Heyfets, A. Israelson, Z. Zaslavsky, T. Bravman, V. Bronner, A. Notcovich, V. Shoshan-Barmatz and E. Flescher, Methyl jasmonate binds to and detaches mitochondria-bound hexokinase, *Oncogene*, 2008, **27**, 4636–4643.

55 C. Combes and C. Rey, Amorphous calcium phosphates: synthesis, properties and uses in biomaterials, *Acta Biomater.*, 2010, **6**, 3362–3378.

56 L. Wang and G. H. Nancollas, Calcium Orthophosphates: Crystallization and Dissolution, *Chem. Rev.*, 2008, **108**, 4628–4669.

57 K. Chatzipanagis, T. Roncal-Herrero, M. Bilton, A. Tampieri, R. Kröger, J. M. Delgado-López and M. Iafisco, Crystallization of citrate-stabilized amorphous calcium phosphate to nanocrystalline apatite: a surface-mediated transformation, *CrystEngComm*, 2016, **18**, 3170–3173.

58 I. Iavicoli, V. Leso, D. H. Beezhold and A. A. Shvedova, Nanotechnology in agriculture: Opportunities, toxicological implications, and occupational risks, *Toxicol. Appl. Pharmacol.*, 2017, **329**, 96–111.

59 D. Reischer, A. Heyfets, S. Shimony, J. Nordenberg, Y. Kashman and E. Flescher, Effects of natural and novel synthetic jasmonates, *Br. J. Pharmacol.*, 2007, **150**, 738–749.

60 J. M. Delgado-López, I. Rodríguez-Ruiz, M. A. Durán-Olivencia, M. Iafisco, A. Tampieri, D. Colangelo, M. Prat and J. Gómez-Morales, pH-Responsive Delivery of Doxorubicin from Citrate–Apatite Nanocrystals with Tailored Carbonate Content, *Langmuir*, 2013, **29**, 8213–8221.

61 Y. Jiang, J. Ye, S. Li and Ü. Niinemets, Methyl jasmonate-induced emission of biogenic volatiles is biphasic in cucumber: A high-resolution analysis of dose dependence, *J. Exp. Bot.*, 2017, **68**, 4679–4694.

This journal is © The Royal Society of Chemistry 2021

Environ. Sci.: Nano, 2021, **8**, 3524–3535 | 3535